THERMODYNAMICS AND MOLECULAR-SCALE PHENOMENA





Reversible ion binding for polyelectrolytes with adaptive conformations

Sean Friedowitz | Jian Qin D

Department of Chemical Engineering, Stanford University, Stanford, California, USA

Correspondence

Jian Qin, Department of Chemical Engineering, Stanford University, Stanford, CA 94305, USA. Email: jianq@stanford.edu

Funding information

National Science Foundation, Grant/Award Number: DMR-1846547; Department of Chemical Engineering at the Stanford University

Abstract

Polyelectrolytes may adopt rod- or coil-like conformations depending on the strength of intrachain repulsion and the effective charge density. The charge density of polyelectrolytes is influenced not only by the binding of small ions, but also by the binding with oppositely charged chains. We introduce a coupled variational approach that treats reversible ion binding, adaptive chain structure, and electrostatic correlations simultaneously. This approach captures the swelling and deswelling of single polyelectrolyte chains, and the competition between interchain cross-linking and ion binding in mixtures of polyelectrolytes. Applying our theory to study polyelectrolyte coacervation, we identify two distinct regimes. In the weak binding regime, the charge density is high and the solution properties are dependent on the conformations of polyelectrolytes. In the strong binding regime, this dependence is weakened and the solution thermodynamics are dominated by the short-range ion-binding equilibrium.

1 | INTRODUCTION

Mixtures of oppositely charged polyelectrolytes in aqueous solution can undergo an associative, liquid-liquid phase separation, yielding a polymer-rich complex in coexistence with a dilute supernatant. The complexes show a continuum of morphological features, ranging from viscous liquid-like fluids, known as coacervates, to solid-like aggregates, ¹⁻³ and may contain microstructured domains. ⁴⁻⁷ Since its initial experimental observation, ⁸ the concentrated coacervates have found applications as therapeutic delivery devices, ^{9,10} advanced adhesives and coatings, ^{11,12} and food processing additives. ^{13,14} More recently, this liquid-phase instability has been recognized as an underlying mechanism that orchestrates intracellular compartmentalization, cellular metabolism, and disease pathogenesis. ¹⁵⁻¹⁷ In this context, understanding the interplay between the specific molecular properties and the stability of polyelectrolyte complexation is necessary.

Polyelectrolyte complexation is governed by a myriad of longand short-range interactions. Long-range electrostatic interactions lead to favorable spatial correlations between oppositely charged species, ¹⁸ which give rise to the characteristic scattering peak in polyelectrolyte solutions. ¹⁹ However, electrostatic effects alone do not account for polyelectrolyte complexation in real systems. Recent calorimetric measurements suggest that the driving force for complexation is entropic, due to the release of bound counterions as ion pairs form between polycations and polyanions. $^{20-22}$ A few models for ion binding have been developed that either treat binding explicitly as reversible chemical reactions, $^{23-26}$ use the transfer matrix to account for cooperativity between bound sites, 27,28 or embed the binding equilibrium at the scaling level. 29 These models can in practice be adapted to treat local effects other than ionic association, including acid-base equilibria for weakly dissociating polyelectrolytes, 30 hydrogen-bonding, and $\pi-\pi$ stacking. 6,17,31

The degree of ion binding depends on the conformational properties of polymers. Unlike simple dilute electrolyte solutions where Debye–Hückel theory is applicable, the spatial extent of polyelectrolyte chains introduces new length scales and modifies the concentration-dependence of the electrostatic screening length.³² One way of describing such connectivity effects is to consider weak composition fluctuations, which depend on polymer conformational statistics, and evaluate the resulting electrostatic free energy using the random phase approximation (RPA).^{33–35} The RPA expression to the free energy explicitly depends on the chain structure factor, and

has a distinct concentration dependence for chains adopting rodlike conformations, coil-like conformations, or conformations with alternative fractal dimensions.³⁵ This leads to different degrees of ion binding for different conformational statistics. We have shown that explicitly accounting for the self-energy of ions is needed for a coherent treatment of chain structure and ion binding, and that more flexible, compact conformations result in a greater degree of ion binding.²⁵

Although the standard RPA approach yields results consistent with prevailing scaling arguments, ³⁶ it neglects the variation of chain conformations with concentration, a salient feature of polyelectrolyte solutions. Polyelectrolytes are rod like in dilute solutions, owing to strong self-repulsions and weak screening, and are coil like in the semidilute and concentrated solutions. Using a fixed, coil-like structure factor in the RPA expression is known to overestimate the electrostatic correlation free energy, which results in vanishingly small supernatant concentrations in coacervation phase diagrams. ³⁷

Earlier theories have considered adaptive structures in polyelectrolyte solutions. The "double-screening" theory allows chain structure to respond to both screened electrostatic and excluded volume interactions, ³⁸ and has been used to study counterion adsorption in single-phase solutions. ^{39–41} It, however, does not describe the interchain binding in solutions containing oppositely charged polyelectrolytes. More recent studies used the variational approach to study polyelectrolyte solution. ^{42–44} The renormalized Gaussian fluctuation (RGF) model self-consistently determines the persistence length in the presence of both polyelectrolyte and salt screening, ⁴³ and has been applied to study coacervation. ⁴⁴ What is missing is the simultaneous treatment of adaptive chain structure and short-range ion binding. The significance of ion binding in regulating the charge density of polyelectrolytes, and in turn their conformational properties, has been stressed in a recent review. ³²

In this work, our previous theory on reversible ion binding^{24,25} is combined with the RGF model⁴³ to describe the adaptive chain stiffness and coacervation behavior. Inspired by Reference 43, we introduce a coupled variational approach that allows for self-consistent determination of the extents of ion binding and the effective chain stiffness, both dictated by electrostatic interactions among charged species. Where applicable, we highlight the role of adaptive chain flexibility by comparison to chains with fixed rod- or coil-like structures.

This article is organized as follows. In Section 2, we develop the model for solutions of a single type of polyion. The coupled variational approach for both ion binding and chain flexibility is presented, and its implications on solution structure are explored. In Section 3, we extend the approach to study polyelectrolyte complex coacervation in solutions of oppositely charged polyions. Interchain binding between polyanions and polycations is explicitly treated. Coacervation phase diagrams are presented for different chain structures, and conditions under which long-range electrostatics or short-range binding dominate coacervation behavior are identified. Our main findings are summarized in Section 4.

2 | SINGLE-POLYELECTROLYTE SOLUTIONS

We begin by studying simple polyelectrolyte solutions containing counterions and added salt. By incorporating the treatment of adaptive chain structure into our previous work²⁵ on ion binding, we show how chain stiffness and solution properties vary with the degree of ion binding, composition, and strength of electrostatic interactions.

2.1 | Free energy for associative polyelectrolyte solutions

We consider an aqueous solution of polyanions of length N_A in the presence of counterions and coions. The numbers of polyanions, cations, and anions are n_A , n_+ , and n_- , and the volume fractions are ϕ_A , ϕ_+ , and ϕ_- , respectively. For simplicity, we assume that all polyanion monomers can be ionized, and monomers, cations, and anions are monovalent. To facilitate unit conversion, a common reference volume $v_0 = 30\,\text{Å}^3$ is chosen for monomers and ions. The molecular volumes v_i (i=A, +, and -) are normalized as $\omega_i = v_i/v_0$. A common length unit $l_0 = v_0^{1/3}$ is also used in the following. For bulk solutions, electroneutrality requires that $n_+ = n_A N_A$ in the absence of added salt or, equivalently, $\phi_+ = \phi_A \omega_+/\omega_A$. If the composition of added salt is ϕ_5 , the volume fractions of cations and anions are $\phi_+ = \phi_A \omega_+/\omega_A + \phi_S$ and $\phi_- = \phi_S$.

At any given composition, a fraction of cations α are bound to polyanions and neutralize their charges. The number of polyanion monomers harboring bound cations is $n_{A+}=\alpha n_A N_A$, the charge density on polyanions is $\sigma_A=1-\alpha$, the volume fraction of bound ions is $\phi_+^b=\alpha\phi_A\omega_+/\omega_A$, and the fraction of free cations is $\phi_+^f=\phi_+-\phi_+^b$. Ion binding can be conceived as a reversible reaction of the form^{24,26}

$$(A) + (+) \stackrel{\Delta G_{A^+}^{eff}}{\rightleftharpoons} (A+), \tag{1}$$

where ΔG_{A+}^{eff} is an effective free energy governing the binding equilibrium. It contains a local contribution denoted ΔG_{A+} and a nonlocal contribution due to electrostatic interactions.

The explicit expression for ΔG_{A+}^{eff} is derived from the solution free energy density f which consists of four additive terms in our model,

$$f = \frac{v_0 F}{V k_B T} = f_{trans} + f_{comb} + f_{bind} + f_{el}.$$
 (2)

The first term f_{trans} is the mixing entropy for all species that can be freely "translated,"

$$f_{\rm trans} = \frac{\phi_{\rm A}}{\omega_{\rm A}N_{\rm A}} \ln(\phi_{\rm A}) + \frac{\phi_+^{\rm f}}{\omega_+} \ln(\phi_+^{\rm f}) + \frac{\phi_-}{\omega_-} \ln(\phi_-) + \phi_{\rm W} \ln(\phi_{\rm W}), \eqno(3)$$

where $\phi_W = 1 - \phi_A - \phi_+ - \phi_-$ is the volume fraction of solvent that enforces the incompressibility constraint. The second term f_{comb} is a

combinatorial factor accounting for the number of ways to pair cations with unbound monomers, which reads^{25,34,39}

$$f_{\text{comb}} = \frac{\phi_{\text{A}}}{\omega_{\text{A}}} [\alpha \ln(\alpha) + (1 - \alpha) \ln(1 - \alpha)]. \tag{4}$$

The third term f_{bind} is the total *local* binding free energy, given by the product between ΔG_{A+} and the fraction of bound ions,

$$f_{\text{bind}} = \frac{\alpha \phi_{\text{A}}}{\omega_{\text{A}}} \Delta G_{\text{A+}}.$$
 (5)

This local term captures the short-range interactions that contribute to the equilibrium of ion binding. $^{24-26}$ It may be attributed to perturbations in water solvation shells upon binding, the local permittivity around bound charge centers, 39 or the chemical details of polyanions and cations. 45 For our purpose, it suffices to treat ΔG_{A+} as a model parameter with value of order k_BT .

The fourth term $f_{\rm el}$ is the electrostatic interaction of the fluctuating charge density, which is treated at the level of RPA.^{25,34,35} The procedure for deriving it is discussed in Appendix S1, and the result is

$$f_{\rm el} = \frac{1}{4\pi^2} \int_0^\infty dq \, q^2 \ln\left(1 + \frac{\kappa^2(q)}{q^2}\right),$$
 (6)

$$\kappa^2(q) \equiv 4\pi I_{\text{B}} \Big(\widetilde{\Omega}_-(q) + \widetilde{\Omega}_+^{\text{f}}(q) + \sigma_{\text{A}}^2 \widetilde{\Omega}_{\text{A}}(q) \Big). \tag{7} \label{eq:partial_problem}$$

Here, the integration is performed over the dimensionless wavenumber q. The dimensionless Bjerrum length is defined as $l_B \equiv e^2/(4\pi e k_B T l_0)$, which defaults to $l_B = 2.29$ for an aqueous solution at room temperature. The term $\kappa(q)$ may be interpreted as the inverse of a wavenumber-dependent screening length.

The factors $\widetilde{\Omega}_i(q)$ are the ideal intramolecular correlation functions for anions, unbound cations, and polyanions, given by

$$\widetilde{\Omega}_{-}(q) = \frac{\phi_{-}}{\omega} \widehat{\Gamma}_{-}^{2}(q), \tag{8}$$

$$\widetilde{\Omega}_{+}^{\mathsf{f}}(q) = \frac{\phi_{+}^{\mathsf{f}}}{\omega_{+}} \widehat{\Gamma}_{+}^{2}(q), \tag{9}$$

$$\widetilde{\Omega}_{A}(q) = \frac{\phi_{A}}{\omega_{A}} N_{A} g_{A}(q) \hat{\Gamma}_{A}^{2}(q). \tag{10}$$

The terms $\hat{\Gamma}_i(q) = \exp(-q^2 a_i^2/2)$ (i = A, +, and -)) are the Fourier transforms of Gaussian smearing functions for point-like charges, with a_i being the smearing width. The smearing functions regularize the high-q divergence of the electrostatic interaction between overlapping point-like charges. For nonassociating systems, such smearing can be avoided by absorbing the divergence into the self-energy of ions, which represents the free energy cost for transferring

isolated ions into the solution.³⁵ For associating systems, explicit inclusion of smearing functions is essential because, not knowing the charge density of each species a priori, removal of the self-energy is impossible.²⁵ Larger values of the smearing widths weaken electrostatic interactions, altering the quantitative results from the model; throughout this work, we set a_i to the radius of the monomers, $a_i = \omega_i^{1/3}/2$.

The polyanion correlation function $\widetilde{\Omega}_A(q)$ describes the conformational properties of the ideal chains through the form factor $g_A(q)$. For Gaussian coils, the form factor is the Debye function $g_D(x) = \frac{2}{x^2}(x-1+e^{-x})$, with $x=q^2R_g^2$ and R_g being the radius of gyration. For rod-like chains, the form factor is the Neugebauer function $g_N(x) = \frac{2}{x}\left(\int_0^x \mathrm{d}t \, \frac{\sin(t)}{t} - \frac{1-\cos(x)}{x}\right)$ with x=qL and L being the backbone length. More general cases for chains with arbitrary internal connectivity have been considered.

In this work, to allow for adaptive chain structures in response to varying degrees of ion binding, we model the polymers as worm-like chains (WLC). Although the exact WLC form factor is known, ^{52,53} to avoid cumbersome algebra, we adopt a form that interpolates the rod- and coil-like behaviors in the short- and long-chain limits, respectively, ^{42,43}

$$g_{A}(q;\ell_{A}) = \frac{e^{-q\ell_{A}/2}}{1 + q^{2}N_{A}b_{A}\ell_{A}/6} + \frac{1 - e^{-q\ell_{A}/2}}{1 + qN_{A}b_{A}/\pi}.$$
 (11)

Here, b_A is the segment length for the polyanions and is set to I_0 in this work. The effective persistence length ℓ_A is a model parameter, which controls the crossover between rod- and coil-like behaviors. Equation (11) reduces to coil-like scaling for small ℓ_A , and to rod-like scaling for large ℓ_A . The value of ℓ_A is found by minimizing the free energy of a single chain subject to screened electrostatic interactions, as described below.

2.2 | Self-consistent treatment of ion binding and chain structure

The two model parameters α and ℓ_A are coupled. The degree of ion binding α depends on the electrostatic contribution to the free energy, which in turn depends on ℓ_A . Reversely, the effective persistence length ℓ_A depends on the strength of intrachain repulsion, ^{43,54,55} which in turn depends on charge density or, identically, α . We thus need to fix these two parameters simultaneously by minimizing the total solution free energy.

Minimizing Equation (2) by setting $\partial f/\partial \alpha = 0$ yields a law of mass action governing the ion binding equilibrium $^{23-26,34,39,56}$

$$K_{A+} \equiv \frac{\alpha}{(1-\alpha)\phi_{i}^{f}} = e^{-\Delta G_{A+} - \mu_{A+}^{gl} + 1},$$
 (12)

in which K_{A+} is the equilibrium constant. This condition amounts to equating the chemical potentials of the free and the bound ions. ²⁶ The sum $\Delta G_{A+} + \mu_{A+}^{el} - 1$ is precisely the effective binding free energy

 $\Delta G_{\rm A+}^{\rm eff}$ introduced in Equation (1). It contains the local contribution $\Delta G_{\rm A}$, and the nonlocal contribution $\mu_{\rm A+}^{\rm el}$ defined by

$$\mu_{\mathsf{A}+}^{\mathsf{el}} \equiv \frac{\omega_{\mathsf{A}}}{\phi_{\mathsf{A}}} \frac{\partial f_{\mathsf{el}}}{\partial \alpha} = -\frac{1}{4\pi^2} \int_0^\infty \mathsf{d}q q^2 \, \widetilde{\mathsf{G}}(q) \Big(\hat{\Gamma}_+^2(q) + 2\sigma_{\mathsf{A}} \mathsf{N}_{\mathsf{A}} \mathsf{g}_{\mathsf{A}} \Big(q; \ell_{\mathsf{A}} \big) \hat{\Gamma}_{\mathsf{A}}^2(q) \Big), \tag{13}$$

where the screened interaction $\widetilde{G}(q)$ is defined as $\widetilde{G}(q) \equiv \frac{4\kappa l_B}{q^2+\kappa^2(q)}$, and $\kappa(q)$ is given by Equation (7). Equation (13) depends on the solution composition, Bjerrum length, degree of ion binding, and chain length and stiffness. It is equal to the difference in the excess chemical potentials of the bound and the free ions, 26 and can be referred to as the electrostatic exchange chemical potential. This term measures the free energy cost of ion binding due to screened electrostatic interactions, or alternatively, the reduction in the self-energy of ions. 25 The structure of the chains influences μ_{A+}^{el} through κ^2 . More flexible, compact chains, corresponding to larger N_A , smaller b_A , or smaller ℓ_A , exhibit greater (more negative) values of μ_{A+}^{el} , particularly in the dilute regime when charges are weakly screened. 25

Equation (12) gives α for a *fixed* chain structure. To optimize the chain structure, we adopt the main result of the RGF theory, 43,44 which expresses the single chain free energy in terms of a sum of the entropic work of deforming the chain F_{ent} , and the screened electrostatic interactions F_{int} . Since both contributions depend on the persistence length ℓ_{A} , we can obtain the optimal value by minimization 43

$$\min_{f} [F_{ent} + F_{int}]. \tag{14}$$

However, unlike the original RGF treatment,⁴³ the optimization over ℓ_A is coupled to the degree of ion binding through the dependence of $F_{\rm int}$ on α . The entropic part in the single-chain free energy was deduced from force-extension relations of semiflexible polymers^{43,57-59}

$$F_{ent} = -\frac{3}{2}N_{A}ln\bigg(1-\frac{\gamma_{A}^{2}}{N_{A}}\bigg) - 3ln(\gamma_{A}). \tag{15} \label{eq:fent}$$

Here, γ_A is the swelling ratio for the mean-squared end-to-end distance defined as $\gamma_A^2 = \frac{\langle R_A^2 \rangle}{\langle R_{AO}^2 \rangle} = 2 \frac{\ell_A}{b_A} \Big[1 - \frac{\ell_A}{N_A b_A} (1 - e^{-N_A b_A / \ell_A}) \Big]$. The value of γ_A ranges from unity at small ℓ_A , corresponding to the ideal, coillike limit, to $N_A^{1/2}$ at infinitely large ℓ_A , for fully extended, rod-like chains. The interaction term accounts for the screened intrachain electrostatic interactions, and has the form⁴³

$$F_{\text{int}} = \frac{1}{4\pi^2} \int_0^\infty dq q^2 \sigma_{A}^2 \widetilde{\Omega}_{A}(q; \ell_A) \widetilde{G}(q), \tag{16}$$

which can be derived by integrating the g_A -dependent term in Equation (13) over α , that is, through a charging process.

Equations (12) and (14) are coupled, and must be solved self-consistently to determine the optimal values of α and ℓ_A , which are then plugged into the solution free energy, Equation (2), to investigate the thermodynamic behavior.

2.3 | Coupling between ion binding and chain swelling

We demonstrate the coupling between ion binding and chain conformation by exploring the effects of polymer concentration and Bjerrum length. For simplicity, in the following, we set the volumes of ions and monomers to v_0 , and use $\omega_i = 1$. Although the local binding free energy ΔG_{A+} is independent of molecular weight, the electrostatic exchange potential Equation (13) is proportional to N_A . Similarly, the RGF self-interaction energy Equation (16) depends on chain length and scales as $N_A \ln(N_A)$ in the rod-like limit.⁴³

Figure 1 shows the variation of the optimal binding fraction and the swelling ratio with polymer concentration for a range of chain

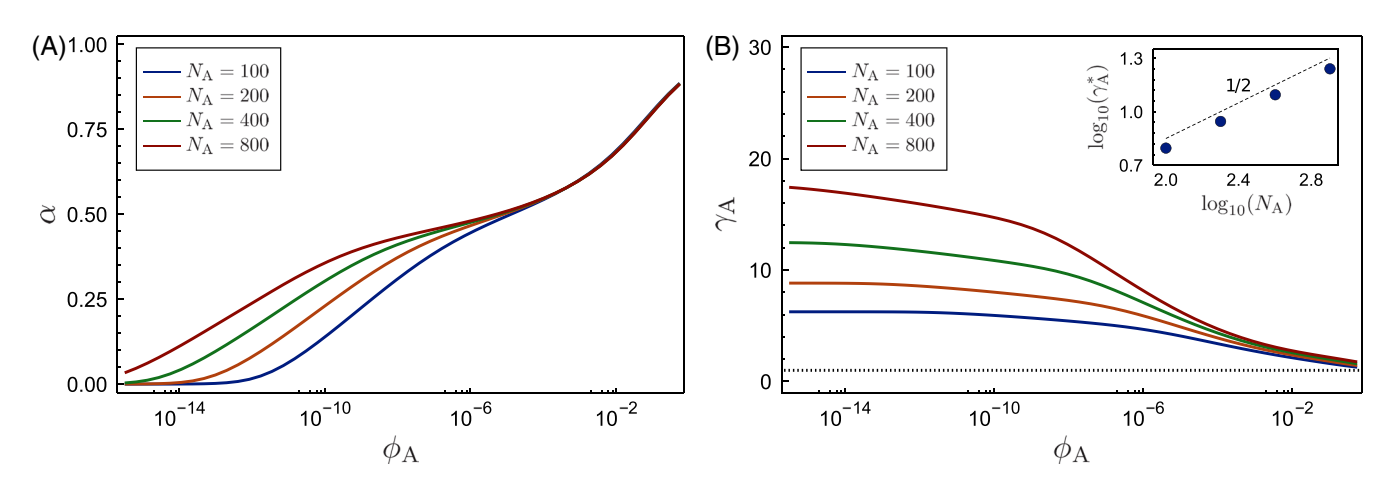


FIGURE 1 Variation of (A) the fraction of bound ions α and (B) the chain expansion factor γ_A with polymer composition and chain length in salt-free solutions. The expansion factor plateaus in the dilute limit. The scaling of the plateau value with molecular weight is shown in the inset of panel (B). Parameters: $\phi_S = 0$, $\Delta G_{A+} = -3$, $b_A = 1$

lengths. Although no extra salt is added ($\phi_{\rm S}=0$), counterions are present in the solution to maintain charge neutrality. The binding fraction α increases with $\phi_{\rm A}$, consistent with the requirement of Le Chatelier's principle. The swelling ratio $\gamma_{\rm A}$ decreases with polymer concentration due to electrostatic screening. Both properties are independent of molecular weight for $\phi_{\rm A} > 10^{-4}$. In this regime, the ratio $\gamma_{\rm A}$ approaches the Gaussian coil limit $\gamma_{\rm A}=1$, and α approaches the asymptotic behavior $\alpha\approx 1-\left(\phi_{+}e^{1-\Delta G_{\rm A+}}\right)^{-1/2}$, since $\mu_{\rm A+}^{\rm el}$ is small when the binding fraction is large (Equation (12)).

The effects of molecular weight are pronounced at low concentrations. The binding fraction drops to zero at sufficient dilution, and the crossover concentration is higher for smaller $N_{\rm A}$ values. The swelling ratio increases with the degree of dilution, and eventually plateaus to an $N_{\rm A}$ -dependent value. The concentration at which the swelling ratio plateaus is higher for smaller $N_{\rm A}$, and is close to the crossover concentration when the binding fraction nearly vanishes. In this limit, chains are fully charged and adopt rod-like conformations. The plateau value of the chain expansion factor $\gamma_{\rm A}^*$ is plotted against molecular weight in the inset of Figure 1B. The scaling $\gamma_{\rm A}^* \sim N_{\rm A}^{1/2}$ affirms rod-like conformations of the chains $(R_{\rm A} \sim N_{\rm A})$.

To further illustrate the coupling between chain expansion and ion binding, we examine the effects of Bjerrum length. A nonmonotonic swelling behavior has been observed in salt-free polyelectrolyte solutions suggesting that, $^{39,60-62}$ with increasing $l_{\rm B}$, flexible polyelectrolytes initially expand due to intrachain repulsions, then collapse at high $l_{\rm B}$ values when a large fraction of ions become bound. This behavior is captured by our model, as shown in Figure 2, for different values of $\Delta G_{\rm A+}$. The initial expansion as $l_{\rm B}$ increases is expected. The collapse for $l_{\rm B} \gtrsim 3$ is caused by the increase in ion binding, as clearly shown in the inset. This type of swelling and deswelling behaviors has been identified in the previous work. 32,39

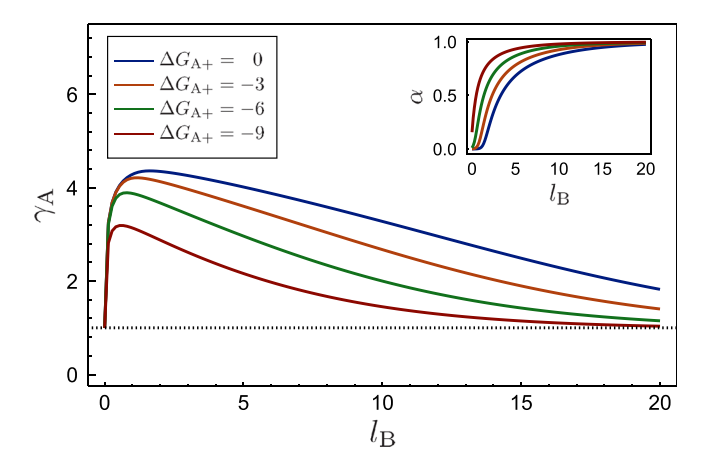


FIGURE 2 Variation of the chain expansion factor γ_A with the Bjerrum length I_B , for different values of binding strength ΔG_{A+} . The degree of ion binding α over the same range of Bjerrum lengths is shown in the inset. Parameters: $\phi_A = 10^{-5}$, $\phi_S = 0$, $N_A = 100$, $b_A = 1$

2.4 | Osmotic pressure

We present results on the osmotic coefficient in this section. To highlight the effects of structural adaptation, we also calculate this property for chains with fixed rod- or coil-like structures. For consistency, we use the interpolated structure factor, Equation (11), for these two reference cases, instead of the Debye or Neugebauer functions. The persistence length ℓ_A is set to $N_A b_A$ for rod-like chains, and to $b_A/2$ for coil-like chains.⁴³

The osmotic pressure of a multicomponent solution is derived from the exchange chemical potentials of solutes $f_i = \partial f/\partial \phi_i$ as $\Pi = \sum_i \phi_i f_i - f = -\mu_W$, where f is the solution free energy and μ_W is the chemical potential of the solvent. The osmotic coefficient is the ratio of Π to the prediction of van't Hoff's law,

$$\Phi = \frac{\Pi}{\sum_{i} \frac{\phi_i}{M}},\tag{17}$$

In the dilute limit, if the excess chemical potential of the solvent is regular, the osmotic coefficient approaches unity. However, due to ion-binding, the osmotic coefficient depends on the binding fraction $\alpha^{.63}$ If we assume the excess chemical potentials $\mu_i^{\rm ex}$ and $\mu_W^{\rm ex}$ decay to zero sufficiently rapidly in the dilute regime, the osmotic pressure can be written $\Pi=\phi_A/N_A+\phi_+^{\rm f}$. In a salt free solution with $\phi_+=\phi_A$, we have $\Phi=1-\frac{aN_A}{1+N_A}$, or $\Phi=1-\alpha$ for long chains. It then follows that the binding free energy and treatment of chain structure affect the limiting value of Φ by modulating the value of α .

The behavior of the osmotic coefficient at higher concentrations has been subject of much discussion. Treating polyelectrolytes as flexible chains at the RPA level produces excessively strong composition fluctuations, resulting in a negative osmotic pressure and thermodynamic instability. Simulations have found that the osmotic coefficient reaches a plateau less than one, and attributed that behavior to the binding of counterions on polymers. Similar behavior has also been predicted by the RGF theory in absence of ion binding, and was rationalized based on the correlation free energy of semidilute rod-like chains.

Figure 3A shows our results for chains of length $N_A=10$ and $N_A=10^6$ respectively. The results for the rod-like and adaptive chains are essentially identical, suggesting that the adaptive chains are adopting rod-like conformations in this concentration range. Further, consistent with previous work, ¹⁹ a dip is found near $\phi_A=0.01$, which is more pronounced for the coil-like case and even becomes negative for $N_A=10^6$. In the dilute limit (within the range explored), the result for Φ for short chains approaches unity, whereas that for the long chains approaches a plateau value less than one.

The plateauing behavior has been reported previously 43,64,65 and, within our model, may be understood by explicitly considering the degree of ion binding (Figure 3B). For concentrations $\phi_{\rm A} > 10^{-4}$, the binding fraction α strongly depends on the value of $\phi_{\rm A}$ and the strength of electrostatic interactions. At lower concentrations, α reaches the limiting values that depend on both chain length and conformation. A positive binding fraction implies that the number of free ions is less

than the stoichiometric value ϕ_+ , which lowers the value of osmotic coefficient. Therefore, a negative correlation is expected between the osmotic coefficient and the binding fraction. For $N_A=10$, the binding fraction $\alpha \to 0$ implies a limiting value of $\Phi=1$. For $N_A=10^6$ and a coil-like structure, the binding fraction $\alpha \to 1$ implies a limiting value of $\Phi=0$. For $N_A=10^6$ with rod-like or adaptive structures, which are nearly indistinguishable, a finite value is found for both α and Φ . The plateau value for the osmotic coefficient is less than the limit $\Phi=1-\alpha\approx0.7$ expected based on van't Hoff's law, which may be attributed to the correlation energy for stiff chains.⁴³

2.5 | Collective structure factor

A notable feature of polyelectrolyte solutions is a scattering peak at a nonzero wavenumber^{19,32,66} in the collective structure

function at dilute and semidilute concentrations. This feature is tied to electrostatic correlations, and the peak wavenumber $q_{\rm m}$ increases with concentration until disappearing in the concentrated regime. By coupling the optimized structure factor with the standard RPA treatment for composition fluctuations, we obtained the collective solution structure factor for all pairs of species among ions, polyions, and the solvent (Appendix S1). Here, only the result on the polymer density–density correlation function, $S_{\rm A}(q) = \langle \delta \rho_{\rm A}(q) \delta \rho_{\rm A}(-q) \rangle$, is presented, which exhibits the salient scattering peak.

Figure 4A shows the results for long chains ($N_A = 10^6$) in the weak binding ($\Delta G_{A+} = 0$) limit, treated using different structural models. Solid, dashed, and dotted lines are results at dilute, intermediate, and concentrated concentrations. Similar to the case of the osmotic coefficient, the results for rod-like and adaptive structures are nearly identical. We focus on the location of the scattering peak,

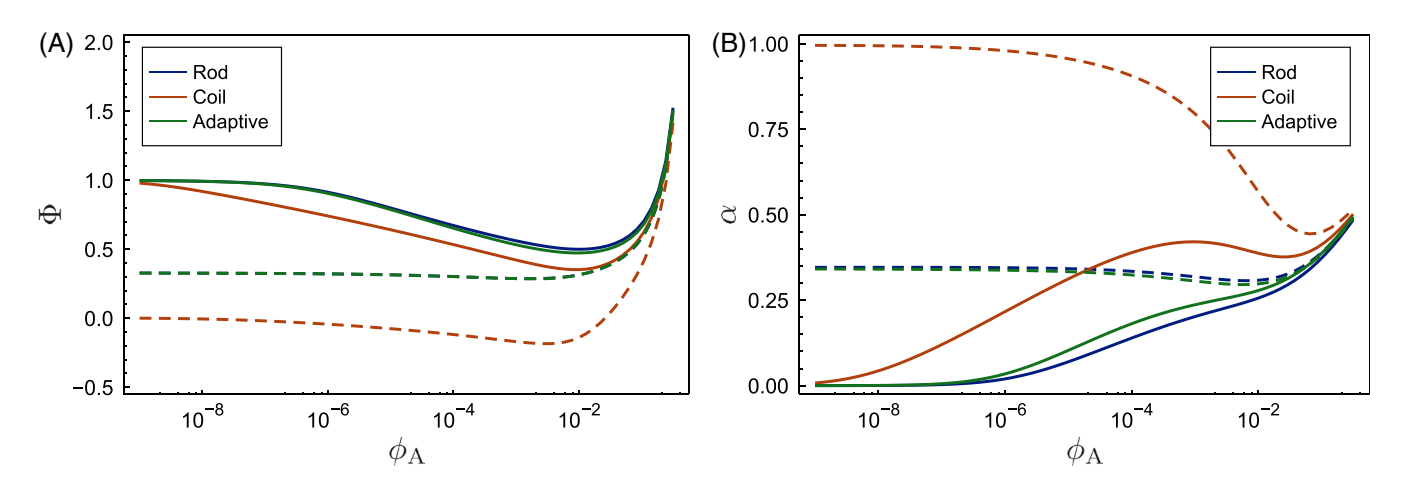


FIGURE 3 Variation of (A) osmotic coefficient Φ and (B) bound ion fraction α with polymer concentration for rod-like, coil-like, and adaptive structures. Solid lines: $N_A = 10$; dashed lines: $N_A = 10^6$. Parameters: $\phi_S = 0$, $\Delta G_{A+} = 0$, $b_A = 1$, $\omega_A = \omega_+ = \omega_- = 1$

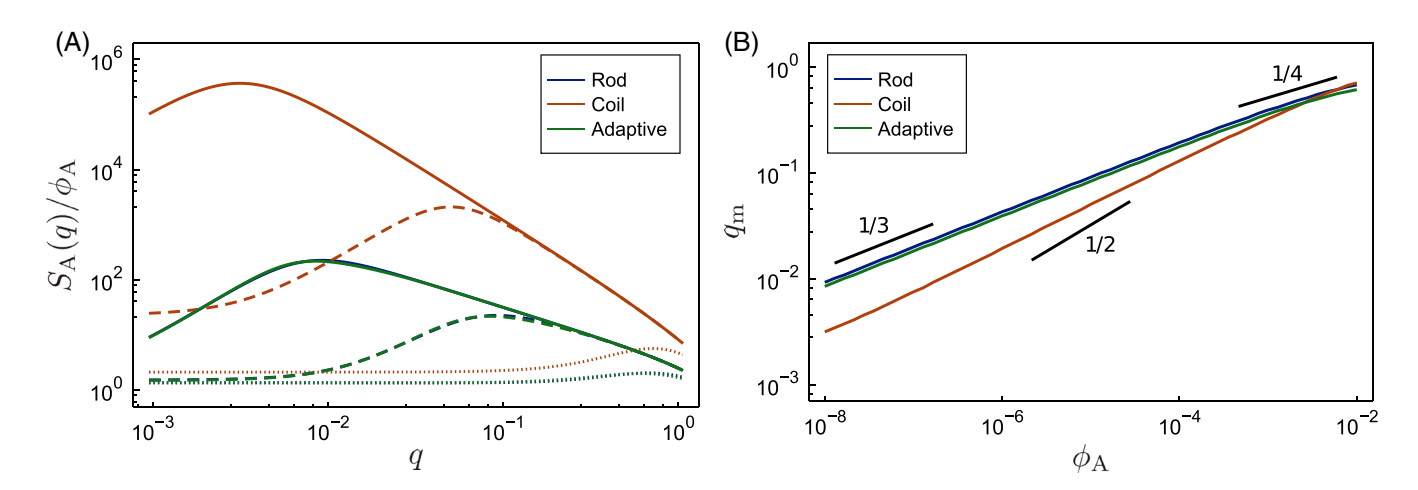


FIGURE 4 Structure factor in salt-free polyelectrolyte solution: (A) variation of polymer-polymer density correlation function S_A with wavenumber q, and (B) variation of peak position q_m with polymer concentration, for rod-like, coil-like, and adaptive structures. In panel (A): $\phi_A = 10^{-8}$ (solid lines), $\phi_A = 10^{-5}$ (dashed lines), and $\phi_A = 10^{-2}$ (dotted lines). Parameters: $\phi_S = 0$, $\Delta G_{A+} = 0$, $N_A = 10^6$, $b_A = 1$, $\omega_A = \omega_+ = \omega_- = 1$

while noting that the peak intensity is higher for the coil-like case and decreases as concentration increases.

The peak position increases with concentration, as shown in Figure 4B. The previous work has suggested that $q_{\rm m} \sim \phi_{\rm A}^{\nu}$ with variable scaling exponent ν : $\nu=1/3$ in the dilute regime, $\nu=1/2$ in the intermediate regime, and $\nu=1/4$ in the concentrated regime. The exponent $\nu=1/3$ is related the interchain distance. The other two scales have been extensively discussed. Our results for coil-like chains obey these scaling relations quite well, though with a slightly smaller exponent at intermediate concentrations. However, no clear crossover between dilute and concentrated scalings is observed for rod-like chains. We posit that this difference in the scaling behavior is related to a general trend we observed, that is, flexible, coil-like chain structures produce too strong an electrostatic correlation at low concentrated scaling to dilute scaling quicker, as their interactions are weaker at low concentration

3 | COACERVATION OF ADAPTIVE CHAINS

In this section, we extend our model to mixtures of polyanions and polycations, and study how adaptive chain structure affects the coacervation of polyions. The treatment of structural adaptation is analogous to that for solutions of single polyelectrolytes. However, since we allow for ion pairing between polyanions and polycations, the combinatorial and electrostatic free energies are different.

3.1 | Free energy with polyanion-polycation binding

We consider a solution consisting of polyanions, polycations, cation, and anions, denoted A, C, (+) and (-), respectively. The volume fractions are $\phi_{\rm A},\,\phi_{\rm C},\,\phi_{-}$, and ϕ_{+} , and the ratios of the volumes of monomers and ions and the common reference are $\omega_{\rm A},\,\omega_{\rm C},\,\omega_{+},$ and ω_{-} . Similar to the previous section, both polyanions and polycations are assumed to be fully ionized. Three types of ion binding are considered, symbolized as 24,26

$$\begin{split} &(A) + (+) \stackrel{\Delta G_{A+}^{eff}}{\rightleftharpoons} (A+), \\ &(C) + (-) \stackrel{\Delta G_{C-}^{eff}}{\rightleftharpoons} (C-), \\ &(A) + (C) \stackrel{\Delta G_{AC}^{eff}}{\rightleftharpoons} (AC). \end{split} \tag{18}$$

In full analogy with Equation (1), the first two lines of the above refer to the binding of polymers with their respective counterions, and the third line refers to the formation of interchain ion pairs between oppositely charged polyions.

The fractions of polyanion or polycation monomer units harboring bound cation or anion are denoted α_{A+} and α_{C-} . The fractions of

polyion monomers that are not bound to small ions but form interchain ion pairs are denoted $\beta_{\rm A}$ and $\beta_{\rm C}$. The net charge densities of the polyions are related to the degrees of ion binding as $\sigma_{\rm A}=(1-\alpha_{\rm A+})(1-\beta_{\rm A})$ and $\sigma_{\rm C}=(1-\alpha_{\rm C-})(1-\beta_{\rm C})$. The fractions of the bound ions are given as $\phi_+^{\rm b}=\alpha_{\rm A+}\phi_{\rm A}\omega_+/\omega_{\rm A}$ and $\phi_-^{\rm b}=\alpha_{\rm C-}\phi_{\rm C}\omega_-/\omega_{\rm C}$. Those of the free ions are then obtained from $\phi_+^{\rm f}=\phi_+-\phi_+^{\rm b}$ and $\phi_-^{\rm f}=\phi_--\phi_-^{\rm b}$. The values of $\alpha_{\rm A+}$, $\alpha_{\rm C-}$, $\beta_{\rm A}$ and $\beta_{\rm C}$ are determined from the equilibrium conditions of the "reactions" in Equation (18), which in turn are governed by a set of reaction free energy changes $\Delta G_{\rm A+}^{\rm eff}$, $\Delta G_{\rm C-}^{\rm eff}$, and $\Delta G_{\rm AC}^{\rm eff}$. Similar to Equation (1), these free energy terms contain both local and long-range electrostatic contributions.

The solution free energy density depends on the stoichiometric composition and the degree of ion binding, and is a sum of four additive terms

$$f = f_{\text{trans}} + f_{\text{comb}} + f_{\text{bind}} + f_{\text{el}}. \tag{19}$$

This decomposition is identical to Equation (2) and is reproduced here for convenience. In general, if the quality of the solvent is needed to fit experimental data, 67,68 a Flory–Huggins free energy term can be added. The first term $f_{\rm trans}$ accounts for the mixing entropy, and is given by

$$\begin{split} f_{\text{trans}} = & \frac{\phi_{\text{A}}}{\omega_{\text{A}} N_{\text{A}}} \ln(\phi_{\text{A}}) + \frac{\phi_{\text{C}}}{\omega_{\text{C}} N_{\text{C}}} \ln(\phi_{\text{C}}) + \frac{\phi_{+}^{\text{f}}}{\omega_{+}} \ln(\phi_{+}^{\text{f}}) + \frac{\phi_{-}}{\omega_{-}} \ln(\phi_{-}) \\ & + \phi_{\text{W}} \ln(\phi_{\text{W}}), \end{split} \tag{20}$$

in which $\phi_{\rm W}$ = 1 - $\phi_{\rm A}$ - $\phi_{\rm C}$ - ϕ_{+} - ϕ_{-} is the volume fraction of solvent.

The second term f_{comb} includes the entropy of arranging both bound small ions and interchain cross-links among monomers on the polyions, and can be further decomposed into three terms, $f_{\text{comb}} = f_{\text{A+}} + f_{\text{C-}} + f_{\text{AC}}$. Here, $f_{\text{A+}}$ and $f_{\text{C-}}$ describe cation binding along the polyanion and anion binding along the polycation,

$$f_{A+} = \frac{\phi_A}{\omega_A} [\alpha_{A+} \ln(\alpha_{A+}) + (1 - \alpha_{A+}) \ln(1 - \alpha_{A+})]. \tag{21}$$

$$f_{C-} = \frac{\phi_C}{\alpha_C} [\alpha_{C-} \ln(\alpha_{C-}) + (1 - \alpha_{C-}) \ln(1 - \alpha_{C-})]. \tag{22}$$

The term f_{AC} arises from the arrangement of ion pairs between the polyelectrolytes and the probability of forming ion pairs, given by, 24,56

$$\begin{split} f_{\mathsf{AC}} &= \frac{(1 - \alpha_{\mathsf{A}+})\phi_{\mathsf{A}}}{\omega_{\mathsf{A}}} [\beta_{\mathsf{A}} \mathsf{ln}(\beta_{\mathsf{A}}) + (1 - \beta_{\mathsf{A}}) \mathsf{ln}(1 - \beta_{\mathsf{A}})] \\ &+ \frac{(1 - \alpha_{\mathsf{C}-})\phi_{\mathsf{C}}}{\omega_{\mathsf{C}}} [\beta_{\mathsf{C}} \mathsf{ln}(\beta_{\mathsf{C}}) + (1 - \beta_{\mathsf{C}}) \mathsf{ln}(1 - \beta_{\mathsf{C}})] \\ &- \frac{\beta_{\mathsf{C}} (1 - \alpha_{\mathsf{C}-})\phi_{\mathsf{C}}}{\omega_{\mathsf{C}}} \mathsf{ln} \bigg(\beta_{\mathsf{C}} (1 - \alpha_{\mathsf{C}-})\phi_{\mathsf{C}} \bigg(\frac{\omega_{\mathsf{A}} + \omega_{\mathsf{C}}}{\omega_{\mathsf{C}}} \bigg) \bigg). \end{split} \tag{23}$$

The first two lines on the right-hand side describe the arrangement of pair-sites on polymers, while the last term accounts for the binding probability.

The third term $f_{\rm bind}$ incorporates specific binding free energies of the reversible charge association reactions, scaled by the fractions of bound ions and respective volume fractions of polyelectrolytes, which is given by

$$f_{bind} = \frac{\alpha_{A+}\phi_A}{\omega_A} \Delta G_{A+} + \frac{\alpha_{C-}\phi_C}{\omega_C} \Delta G_{C-} + \frac{(1-\alpha_{C-})\beta_C\phi_C}{\omega_C} \Delta G_{AC}. \tag{24}$$

We stress that while each binding free energy above (ΔG_{A+} , ΔG_{C-} , or ΔG_{AC}) captures the local interactions around bound charges, the extents of association reactions also depend on the long-range, particularly electrostatic, interactions.

The final contribution to the free energy, $f_{\rm el}$, is due to long-range electrostatic correlations, and again treated at the RPA level. This is given as

$$f_{el} = \frac{1}{4\pi^2} \int_0^\infty dq \ q^2 \ln\left(1 + \frac{\kappa^2(q)}{q^2}\right),$$
 (25)

and is formally identical to Equation (6), although the inverse screening length $\kappa(q)$ now contains the structure factor contribution $\widetilde{\Omega}_C$ from the polycations. Both polyanions and polycations are described by interpolated WLC form factors, Equation (11), with respective persistence lengths ℓ_A and ℓ_C . The dependence on the interchain ion pairing in f_{el} is solely through the effective charge density of the chains. Intermolecular correlations that depend on the network structure of cross-linked polymers $^{23.69}$ are neglected.

3.2 | Coupled binding equilibrium and adaptive chain structures

The variables capturing the degrees of ion binding, α_{A+} , α_{C-} , β_A , and β_C , and those capturing the stiffness of chains, ℓ_A and ℓ_C , are determined following a procedure similar to Section 2. If we mandate that ion pairing occurs under 1:1 stoichiometry, β_A and β_C are related by

$$\frac{\phi_{\rm A}}{\omega_{\rm A}}(1-\alpha_{\rm A+})\beta_{\rm A} = \frac{\phi_{\rm C}}{\omega_{\rm C}}(1-\alpha_{\rm C-})\beta_{\rm C}. \tag{26}$$

Minimizing the free energy with respect to the binding variables, subject to the above constraint, yields a set of coupled laws of mass action:

$$\mathsf{K}_{\mathsf{A}+} \equiv \frac{\alpha_{\mathsf{A}+}}{(1-\beta_{\mathsf{A}})(1-\alpha_{\mathsf{A}+})\phi_{\mathsf{+}}^{\mathsf{f}}} = e^{-\Delta\mathsf{G}_{\mathsf{A}+}-\mu_{\mathsf{A}+}^{\mathsf{cl}}+1}, \tag{27}$$

$$K_{C-} \equiv \frac{\alpha_{C-}}{(1 - \beta_C)(1 - \alpha_{C-})\phi_-^f} = e^{-\Delta G_{C-} - \mu_{C-}^{el} + 1}, \tag{28}$$

$$K_{AC} \equiv \frac{\beta_{A}\omega_{C}}{(1 - \beta_{A})(1 - \beta_{C})(1 - \alpha_{C-})\phi_{C}(\omega_{A} + \omega_{C})} = e^{-\Delta G_{AC} - \mu_{AC}^{el} + 1}. \quad (29)$$

Above, K_{A+} , K_{C-} and K_{AC} are analogous to Equation (12). The interchain binding constant K_{AC} is expressed in terms of ϕ_C , which can be equivalently written in terms of ϕ_A using the stoichiometry constraint, Equation (26). The electrostatic exchange potentials appearing in Equations (27)–(29) are operationally defined as

$$\mu_{A+}^{el} = \frac{\omega_A}{\phi_A} \frac{\partial f_{el}}{\partial \alpha_{A+}},\tag{30}$$

$$\mu_{\mathrm{C-}}^{\mathrm{el}} = \frac{\omega_{\mathrm{C}}}{\phi_{\mathrm{C}}} \frac{\partial f_{\mathrm{el}}}{\partial \alpha_{\mathrm{C-}}},\tag{31}$$

$$\mu_{\mathsf{AC}}^{\mathsf{el}} = \frac{\omega_{\mathsf{C}}}{\phi_{\mathsf{C}}} \frac{\partial f_{\mathsf{el}}}{\partial \beta_{\mathsf{C}}}.\tag{32}$$

The full expressions are given in Appendix S1. Their contributions to the binding equilibrium are included in the "effective" binding free energies introduced in Equation (18), that is, $\Delta G_i^{eff} \equiv \Delta G_i + \mu_i^{el} - 1$ for i = (A+), (C-), (AC).

The laws of mass action defined above can be solved directly for chains with fixed structure in order to determine ion binding extents and calculate coacervation phase diagrams.^{24,26,68} To incorporate adaptive chain stiffness, we use the same variational approach as in Section 2. The optimal persistence lengths for the polyanions and polycations are obtained by minimizing the chain deformation free energies, that is.

$$\min_{\ell_{\Delta}} [F_{\text{ent,A}} + F_{\text{int,A}}], \tag{33}$$

$$\min_{\ell_C} [F_{\text{ent,C}} + F_{\text{int,C}}]. \tag{34}$$

Here, the entropic and interaction contributions are identical to Equation (15) and Equation (16), once the appropriate molecular parameters for polyanions and polycations are substituted.

The above laws of mass action (Equations (27–29)), the conditions for optimal chain persistence length (Equations (33) and (34)), and the ion pairing stoichiometry constraint represent six coupled, nonlinear equations to be solved self-consistently for any given composition and model parameters. The same feedback between ion binding and chain flexibility discussed in Section 2 is expected here—coulombic interactions drive chain expansion through $F_{\rm int,C}$, and promotes ion binding through the electrostatic exchange potentials $\mu_i^{\rm el}$. The resulting interplay of these effects is explored below.

3.3 | Coacervation phase diagrams

We follow the literature^{70,71} to determine the coexistence condition between the supernatant phase, denoted phase 1, and the polymerrich coacervate phase, denoted phase 2. It amounts to equating the osmotic pressure and the exchange electrochemical potentials of the cations, anions, polycations, and polyanions, that is, $\Pi^{(1)} = \Pi^{(2)}$ and $f_i^{(1)} = f_i^{(2)} + \sigma_i \Psi/\omega_i$, (i = A, C, +, -). Here $f_i \equiv \partial f/\partial \phi_i$, and Ψ is the Galvani potential needed to ensure charge neutrality.⁷⁰ This approach is equivalent to the standard common-tangent construction.

To specify the compositions of the two coexisting phases for a given bulk composition $\phi_i^{(0)}$, 10 variables must be fixed: 8 compositions, $\phi_i^{(1)}$ and $\phi_i^{(2)}$, the Galvani potential Ψ , and mass ratio of the two phases ν . The 10 equations needed include five conditions on the osmotic pressure and the exchange electrochemical potentials introduced above, two charge neutrality conditions in both phases, and three independent mass-balance conditions, $\phi_i^{(0)} = (1-\nu)\phi_i^{(1)} + \nu\phi_i^{(2)}$. These equations are solved using Newton's method. Mapping out the coexisting compositions while screening the amount of added salt, analogous to the procedures used in experiment, ⁶⁸ generates the binodal diagrams.

The additional challenge in our model is that the laws of mass action, Equations (27)–(29), need to be solved to determine the binding parameters α_{A+} , α_{C-} , β_A , and β_C , and that the chain deformation free energies, Equations (33) and (34), need to be minimized to determine the persistence lengths ℓ_A and ℓ_C . These inner optimizations are embedded into the free energy calculations for both the supernantant and coacervate phases, allowing for simultaneous determination of binding equilibrium, chain flexibility, and phase coexistence.

To highlight the effects of the ion binding equilibrium and adaptive chain structure on coacervation behavior, we consider solutions that are symmetric in cations and anions, and in polycations and polyanions. Figure 5 shows the binodal diagrams for solutions with $N_A=N_C=100$, $\omega_A=\omega_C=5$, and $\omega_+=\omega_-=1$, over a range of binding free energies. The segment lengths are set to $b_A=\omega_A^{1/3}$ and $b_C=\omega_C^{1/3}$. The reference curves with fixed structures are obtained with constant persistence lengths $\ell_i=N_ib_i$ and $\ell_i=b_i/2$ (i=A,C) for rod- and coillike chains. The values of binding free energies are given in the figure caption. In all cases, we set $\Delta G_{A+}+\Delta G_{C-}=\Delta G_{AC}$, which does not penalize or promote interchain binding at the cost of small ion binding. 1,22,26,45 Evidently, this set of symmetric parameters implies that $\alpha=\alpha_{A+}=\alpha_{C-}$, $\beta=\beta_A=\beta_C$ and, consequently, $\sigma=\sigma_A=\sigma_C$.

In the weak binding case, the binodal curves in Figure 5A show a clear dependence on chain conformation. The results for the adaptive and rod-like chains are nearly indistinguishable, whereas those for the

coil-like chains show a wider two-phase window, in accordance with our results in Section 2 and with the literature.⁴⁴ The inset shows that, for the coil-like chains, the polymer concentration in the supernantant is orders of magnitude lower than the rod-like counterparts, which is consistent with predictions of the RPA theory.³⁷ However, the polymer concentrations in the supernatant phase calculated for coil-like, rod-like, or adaptive chains are far lower than experimental values.^{67,68}

As the binding strength is increased, the two-phase window widens and, more interestingly, the differences in binodal curves calculated using the three chain structures diminish, as shown in Figure 5B,C. To understand this behavior, we examine the degree of ion binding α and interchain ion pairing β along the coexistence curves. The results for the adaptive chains, calculated using the same set of binding parameters as in Figure 5, are plotted against the concentration of the added salt in Figure 6. Similar results for the rod- and coil-like chains are shown in Figure S1. We find that overall the degree of binding increases as the binding strength increases, and that the values of α are greater in the supernatant than the coacervate, whereas the reverse is true for the interchain binding fraction β . Moreover, α progressively increases with increasing salt concentration while β decreases, implying that interchain cross-links are displaced with adsorbed small ions. 1,45

From the binding curves shown in Figure 6, the charge density of the polyelectrolytes can be calculated using $\sigma = (1 - \alpha)(1 - \beta)$. The results are shown in Figure 7 for the model with adaptive chains (the results for rod-like and coil-like chains can be found in Figure S2). With weak binding energies, the charge densities fall in the range of $\sigma \approx 0.5 - 0.8$ for both phases. With stronger binding energies, the charge densities decrease and drop to nearly zero eventually, regardless of chain structure. As the charge density decreases, the electrostatic contribution to the free energy Equation (25) also decreases, which further reduces the electrostatic contribution to the binding equilibrium (Figure S3). On the other hand, the local binding contribution Equation (24) scales with the binding energies. Therefore, in the strong binding regime, the solution free energy is dominated by the local binding contributions, the electrostatic correlation term diminishes, and the chain conformational properties become irrelevant, as shown in Figure 5C.

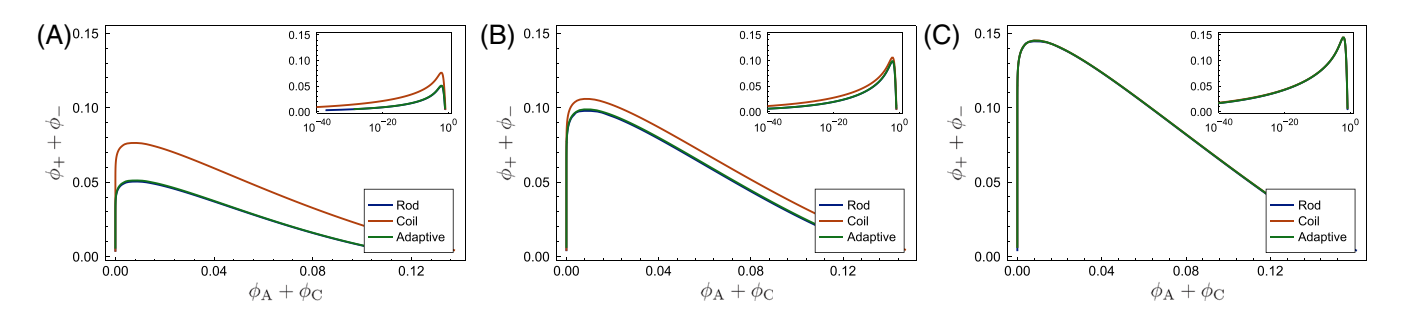


FIGURE 5 Coacervation phase diagrams for symmetric solutions in the salt (y axis) vs. polymer (x axis) plane. The binding parameters are chosen such that $\Delta G_{A+} = \Delta G_{C-}$ and $\Delta G_{A+} + \Delta G_{C-} = \Delta G_{AC}$, with (A) $\Delta G_{AC} = -2$, (B) $\Delta G_{AC} = -4$, and (C) $\Delta G_{AC} = -8$. Parameters: $N_A = N_C = 100$, $\omega_A = \omega_C = 5$, $\omega_+ = \omega_- = 1$

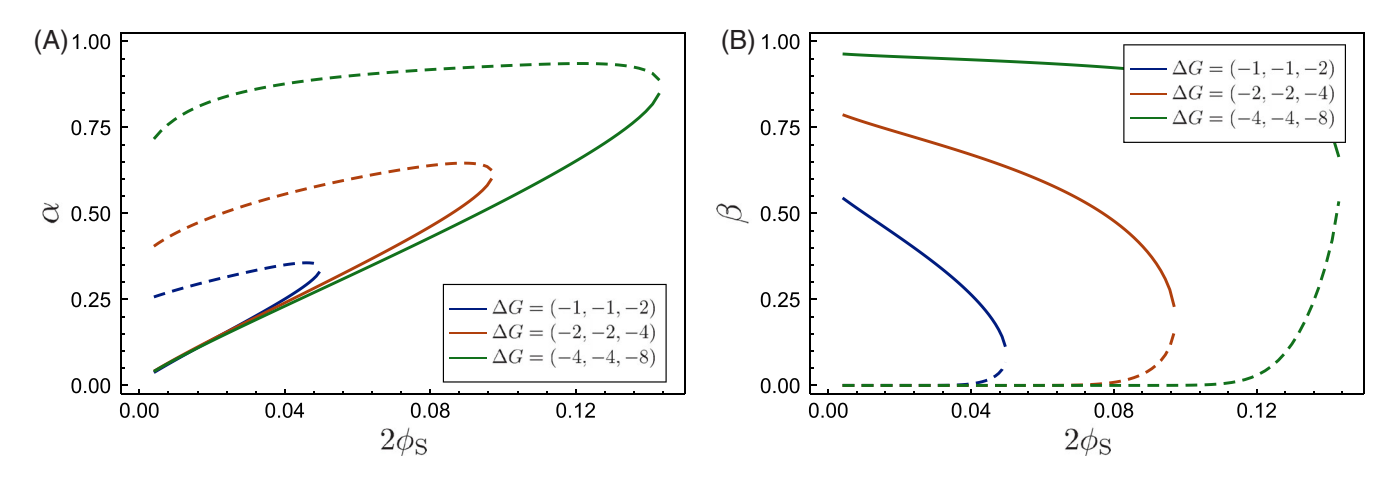


FIGURE 6 Degree of (A) small ion adsorption and (B) interchain ion pairing for chains with adaptive structures along the supernatant branch (dashed lines) and coacervate branch (solid lines) of the phase diagrams shown in Figure 5

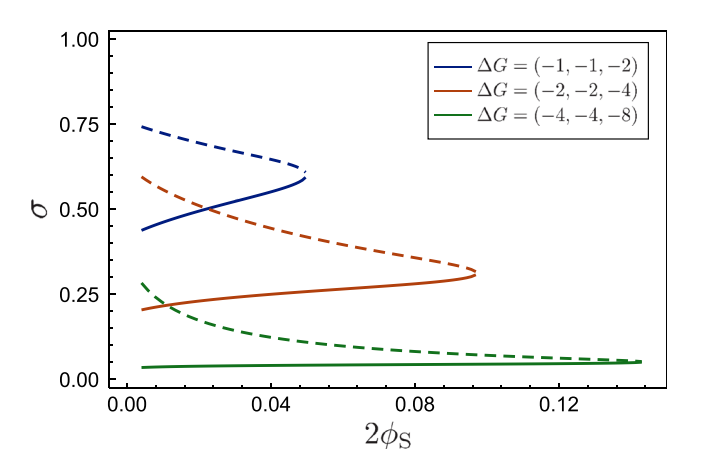


FIGURE 7 Effective charge density for chains with adaptive structures along the supernatant branch (dashed lines) and coacervate branch (solid lines) of the phase diagrams shown in Figure 5

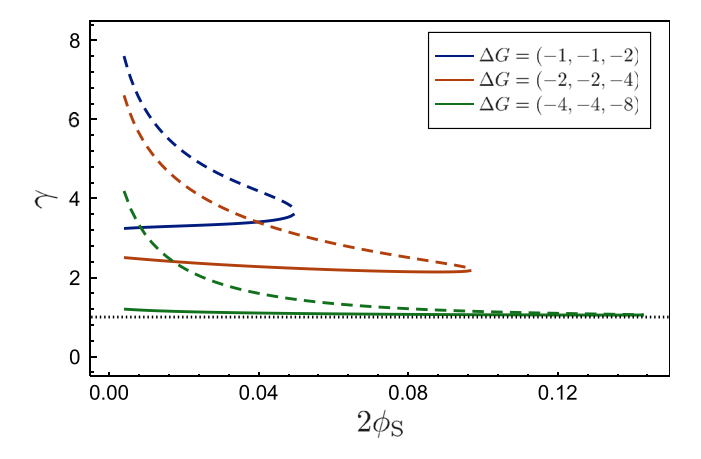


FIGURE 8 Expansion factor for chains with adaptive structures along the supernatant branch (dashed lines) and coacervate branch (solid lines) of the phase diagrams shown in Figure 5

The above argument is further corroborated by examining the swelling behavior of polymers. Figure 8 shows the expansion factors ($\gamma=\gamma_A=\gamma_C$) for different binding strengths. In all cases, the expansion factor is higher in the supernatant phase because it is more dilute, in agreement with prior results from the RGF theory. ⁴⁴ For weak binding, it is clear that chains are strongly expanded in both phases. With increasing binding strength, the chain expansion factor decreases, and approaches unity in the strongly binding limit, particularly in the coacervate branch at high salt concentrations. This is a result of the greatly reduced charge density and electrostatic intrachain repulsion.

4 | CONCLUSIONS

We introduced a model for polyelectrolyte solutions that treats ion binding, interchain binding, and adaptive chain structure simultaneously. The model captures chain expansion in dilute solutions and the nonmonotonic dependence on the Bjerrum length, in accordance with the previous theoretical results. ^{39,43} We found that, over a wide range of solution compositions, the behavior of polyelectrolytes with adaptive chain structures is similar to those with fixed rod-like structures, including the osmotic coefficient (Figure 3), the collective structure factor (Figure 4), and the coacervation phase diagrams (Figure 5). It suggests that the rod-like theory can be used in place of the adaptive theory for practical calculation, especially for long chains.

Two regimes in coacervation behavior were identified, depending on the strength of local ion binding. In the weak binding regime, the charge density of the polyelectrolytes is high, resulting in strong electrostatic interactions. The width of the coacervation window for more flexible, coil-like chains is wider than for stiff, rod-like chains. In the strong binding regime, polyelectrolytes tend to be neutralized by either counterions or chains carrying opposite charges, resulting in weak electrostatic correlations and a minor dependence on chain structure. This regime is similar to that predicted by transfer matrix formalism for strongly correlated, short-range binding. The simultaneous treatment of ion-binding and interchain binding allows us to

AICHE 11 of 12

examine the competitive charge association, which supports the importance of ion-release mechanism, but also points to the importance of interchain crosslinking.

Several approximations are made in our model. The single chain structure is described using an interpolated form factor, Equation (11). The exact WLC structure factor ^{52,53} may be used, but is not expected to change the qualitative conclusions. More severe is the neglect of the structural correlations of cross-linked polymers (i.e., clusters), which may in part be responsible for the significant under-prediction ^{32,37,44} of the polymer concentration in the supernatant phase. ^{67,68} We will expand our theory by incorporating these effects in the future.

ACKNOWLEDGMENTS

This research has been supported by the National Science Foundation CAREER Award through DMR-1846547, and by the startup fund from the Department of Chemical Engineering at the Stanford University.

DATA AVAILABILITY STATEMENT

Research data are not shared.

ORCID

Jian Qin https://orcid.org/0000-0001-6271-068X

REFERENCES

- Wang Q, Schlenoff JB. The polyelectrolyte complex/coacervate continuum. Macromolecules. 2014;47:3108-3116.
- Fares HM, Ghoussoub YE, Delgado JD, Fu J, Urban VS, Schlenoff JB.
 Scattering neutrons along the polyelectrolyte complex/coacervate continuum. *Macromolecules*. 2018;51:4945-4955.
- Tirrell M. Polyelectrolyte complexes: fluid or solid? ACS Cent Sci. 2018;4:532-533.
- Krogstad DV, Lynd NA, Choi S-H, et al. Effects of polymer and salt concentration on the structure and properties of triblock copolymer coacervate hydrogels. *Macromolecules*. 2013;46:1512-1518.
- Audus DJ, Gopez JD, Krogstad DV, et al. Phase behavior of electrostatically complexed polyelectrolyte gels using an embedded fluctuation model. Soft Matter. 2015;11:1214-1225.
- Horn J, Kapelner R, Obermeyer A. Macro- and microphase separated protein-polyelectrolyte complexes: design parameters and current progress. *Polymers*. 2019;11:578.
- Ong GMC, Sing CE. Mapping the phase behavior of coacervate-driven self-assembly in diblock copolyelectrolytes. Soft Matter. 2019;15: 5116-5127.
- 8. Bungenberg de Jong HG, Kruyt H. Coacervation (partial miscibility in colloid systems). *Proc K Ned Akad Wet*. 1929;32:849-856.
- Zhang M, Xiong Q, Wang Y, et al. A well-defined coil-comb polycationic brush with "star polymers" as side chains for gene delivery. Polym Chem. 2014;5:4670-4678.
- Black KA, Priftis D, Perry SL, Yip J, Byun WY, Tirrell M. Protein encapsulation via polypeptide complex coacervation. ACS Macro Lett. 2014; 3:1088-1091.
- Stewart RJ. Protein-based underwater adhesives and the prospects for their biotechnological production. Appl Microbiol Biotechnol. 2010; 89:27-33.
- Stewart RJ, Wang CS, Shao H. Complex coacervates as a foundation for synthetic underwater adhesives. Adv Colloid Interface Sci. 2011; 167:85-93.

- 13. Turgeon S, Schmitt C, Sanchez C. Protein–polysaccharide complexes and coacervates. *Curr Opin Colloid Interface Sci.* 2007;12:166-178.
- Schmitt C, Turgeon SL. Protein/polysaccharide complexes and coacervates in food systems. Adv Colloid Interface Sci. 2011;167:63-70.
- Brangwynne CP, Tompa P, Pappu RV. Polymer physics of intracellular phase transitions. *Nat Phys.* 2015;11:899-904.
- Shin Y, Brangwynne CP. Liquid phase condensation in cell physiology and disease. Science. 2017;357:eaaf4382.
- Bracha D, Walls MT, Brangwynne CP. Probing and engineering liquidphase organelles. Nat Biotechnol. 2019;37:1435-1445.
- Michaeli I, Overbeek JTG, Voorn MJ. Phase separation of polyelectrolyte solutions. J Polym Sci. 1957;23:443-450.
- Muthukumar M. Electrostatic correlations in polyelectrolyte solutions. Polym Sci Ser A. 2016;58:852-863.
- Laugel N, Betscha C, Winterhalter M, Voegel J-C, Schaaf P, Ball V. Relationship between the growth regime of polyelectrolyte multilayers and the polyanion/polycation complexation enthalpy. *J Phys Chem B*. 2006;110:19443-19449.
- Fu J, Schlenoff JB. Driving forces for oppositely charged polyion association in aqueous solutions: Enthalpic, entropic, but not electrostatic. J Am Chem Soc. 2016;138:980-990.
- Schlenoff JB, Yang M, Digby ZA, Wang Q. Ion content of polyelectrolyte complex coacervates and the donnan equilibrium. *Macromolecules*. 2019;52:9149-9159.
- Kudlay A, Ermoshkin AV, de la Cruz MO. Complexation of oppositely charged polyelectrolytes: effect of ion pair formation. *Macromolecules*. 2004;37:9231-9241.
- Salehi A, Larson RG. A molecular thermodynamic model of complexation in mixtures of oppositely charged polyelectrolytes with explicit account of charge association/ dissociation. *Macromolecules*. 2016; 49:9706-9719.
- Friedowitz S, Salehi A, Larson RG, Qin J. Role of electrostatic correlations in polyelectrolyte charge association. J Chem Phys. 2018;149: 163335.
- Ghasemi M, Friedowitz S, Larson RG. Analysis of partitioning of salt through doping of polyelectrolyte complex coacervates. *Macromole*cules. 2020;53:6928-6945.
- Lytle TK, Sing CE. Transfer matrix theory of polymer complex coacervation. Soft Matter. 2017;13:7001-7012.
- Lytle TK, Sing CE. Tuning chain interaction entropy in complex coacervation using polymer stiffness, architecture, and salt valency. Mol Syst Des Eng. 2018;3:183-196.
- 29. Danielsen SPO, Panyukov S, Rubinstein M. Ion pairing and the structure of gel coacervates. *Macromolecules*. 2020;53:9420-9442.
- Ghasemi M, Larson RG. Role of electrostatic interactions in charge regulation of weakly dissociating polyacids. *Prog Polym Sci.* 2021;112: 101322.
- Boeynaems S, Holehouse AS, Weinhardt V, et al. Spontaneous driving forces give rise to protein-RNA condensates with coexisting phases and complex material properties. *Proc Natl Acad Sci.* 2019;116:7889-7898.
- Muthukumar M. 50th anniversary perspective: a perspective on polyelectrolyte solutions. *Macromolecules*. 2017;50:9528-9560.
- Borue VY, Erukhimovich IY. A statistical theory of weakly charged polyelectrolytes: fluctuations, equation of state and microphase separation. *Macromolecules*. 1988;21:3240-3249.
- Ermoshkin AV, de la Cruz MO. A modified random phase approximation of polyelectrolyte solutions. *Macromolecules*. 2003;36:7824-7832.
- Qin J, de Pablo JJ. Criticality and connectivity in macromolecular charge complexation. Macromolecules. 2016;49:8789-8800.
- Rumyantsev AM, Zhulina EB, Borisov OV. Complex coacervate of weakly charged polyelectrolytes: diagram of state. *Macromolecules*. 2018;51:3788-3801.

- Delaney KT, Fredrickson GH. Theory of polyelectrolyte complexation complex coacervates are self-coacervates. J Chem Phys. 2017;146: 224902
- Muthukumar M. Double screening in polyelectrolyte solutions: limiting laws and crossover formulas. J Chem Phys. 1996;105:5183-5199.
- Muthukumar M. Theory of counter-ion condensation on flexible polyelectrolytes: adsorption mechanism. J Chem Phys. 2004;120:9343-9350.
- Kundagrami A, Muthukumar M. Theory of competitive counterion adsorption on flexible polyelectrolytes: divalent salts. J Chem Phys. 2008:128:244901.
- 41. Kumar R, Kundagrami A, Muthukumar M. Counterion adsorption on flexible polyelectrolytes: comparison of theories. *Macromolecules*. 2009;42:1370-1379.
- Ermoshkin AV, Kudlay AN, de la Cruz MO. Thermoreversible crosslinking of polyelectrolyte chains. J Chem Phys. 2004;120:11930-11940
- 43. Shen K, Wang Z-G. Electrostatic correlations and the polyelectrolyte self energy. *J Chem Phys.* 2017;146:084901.
- 44. Shen K, Wang Z-G. Polyelectrolyte chain structure and solution phase behavior. *Macromolecules*. 2018;51:1706-1717.
- Fu J, Fares HM, Schlenoff JB. Ion-pairing strength in polyelectrolyte complexes. Macromolecules. 2017;50:1066-1074.
- 46. Wang Z-G. Fluctuation in electrolyte solutions: the self energy. *Phys Rev* E. 2010:81:021501. https://doi.org/10.1103/physreve.81.021501
- 47. Villet MC, Fredrickson GH. Efficient field-theoretic simulation of polymer solutions. *J Chem Phys.* 2014;141:224115.
- 48. Grzetic DJ, Delaney KT, Fredrickson GH. The effective χ parameter in polarizable polymeric systems: one-loop perturbation theory and field-theoretic simulations. *J Chem Phys.* 2018;148:204903.
- 49. Debye P. Molecular-weight determination by light scattering. *J Phys Colloid Chem.* 1947;51:18-32.
- 50. de Gennes PG. Theory of long-range correlations in polymer melts. Faraday Discuss Chem Soc. 1979;68:96.
- Neugebauer T. Berechnung der lichtzerstreuung von fadenkettenlösungen. Ann Phys. 1943;434:509-533.
- 52. Spakowitz AJ, Wang Z-G. Exact results for a semiflexible polymer chain in an aligning field. *Macromolecules*. 2004;37:5814-5823.
- Zhang X, Jiang Y, Miao B, Chen Y, Yan D, Chen JZY. The structure factor of a wormlike chain and the random-phase-approximation solution for the spinodal line of a diblock copolymer melt. Soft Matter. 2014;10:5405-5416.
- Dobrynin AV. Electrostatic persistence length of semiflexible and flexible polyelectrolytes. *Macromolecules*. 2005;38:9304-9314.
- Fixman M. Electrostatic persistence length. J Phys Chem B. 2010;114: 3185-3196.
- Semenov AN, Rubinstein M. Thermoreversible gelation in solutions of associative polymers. 1. Statics. Macromolecules. 1998;31:1373-1385.
- 57. Marko JF, Siggia ED. Stretching DNA. *Macromolecules*. 1995;28: 8759-8770.

- Jha PK, Solis FJ, de Pablo JJ, de la Cruz MO. Nonlinear effects in the nanophase segregation of polyelectrolyte gels. *Macromolecules*. 2009; 42:6284-6289
- Yang D, Wang Q. Unified view on the mean-field order of coilglobule transition. ACS Macro Lett. 2013;2:952-954.
- Winkler RG, Gold M, Reineker P. Collapse of polyelectrolyte macromolecules by counterion condensation and ion pair formation: a molecular dynamics simulation study. *Phys Rev Lett.* 1998;80:3731-3734.
- Liu S, Muthukumar M. Langevin dynamics simulation of counterion distribution around isolated flexible polyelectrolyte chains. J Chem Phys. 2002;116:9975-9982.
- Loh P, Deen GR, Vollmer D, et al. Collapse of linear polyelectrolyte chains in a poor solvent: when does a collapsing polyelectrolyte collect its counterions? *Macromolecules*. 2008;41:9352-9358.
- 63. Dobrynin AV, Rubinstein M. Theory of polyelectrolytes in solutions and at surfaces. *Prog Polym Sci.* 2005;30:1049-1118.
- Liao Q, Dobrynin AV, Rubinstein M. Molecular dynamics simulations of polyelectrolyte solutions: osmotic coefficient and counterion condensation. *Macromolecules*. 2003;36:3399-3410.
- Carrillo J-MY, Dobrynin AV. Polyelectrolytes in salt solutions: molecular dynamics simulations. *Macromolecules*. 2011;44:5798-5816.
- Nishida K, Kaji K, Kanaya T. High concentration crossovers of polyelectrolyte solutions. J Chem Phys. 2001;114:8671-8677.
- Spruijt E, Westphal AH, Borst JW, Stuart MAC, van der Gucht J. Binodal compositions of polyelectrolyte complexes. *Macromolecules*. 2010;43:6476-6484.
- Lou J, Friedowitz S, Qin J, Xia Y. Tunable coacervation of well-defined homologous polyanions and polycations by local polarity. ACS Cent Sci. 2019;5:549-557.
- Ermoshkin AV, Cruz MODL. Gelation in strongly charged polyelectrolytes. J Polym Sci B. 2004;42:766-776.
- Zhang P, Alsaifi NM, Wu J, Wang Z-G. Salting-out and salting-in of polyelectrolyte solutions: a liquid-state theory study. *Macromolecules*. 2016;49:9720-9730.
- Zhang P, Alsaifi NM, Wu J, Wang Z-G. Polyelectrolyte complex coacervation: effects of concentration asymmetry. *J Chem Phys.* 2018; 149:163303.

SUPPORTING INFORMATION

Additional supporting information may be found in the online version of the article at the publisher's website.

How to cite this article: Friedowitz S, Qin J. Reversible ion binding for polyelectrolytes with adaptive conformations. *AIChE J.* 2021;e17426. doi:10.1002/aic.17426